Supporting Information

Nonlinear optical properties of porphyrin-based covalent organic frameworks determined by steric-orientation of conjugation

Bin Liang,[a,c] Jie Zhao, [c] Jingjing Wang,[c] Yunfei Li,[c] Bin Han,[b] Jie Li,*[a] Xu Ding,*[b] Zheng Xie,*[c] Hailong Wang,[b] and Shuyun Zhou [c]

a. Key Laboratory of Interface Science and Engineering in Advanced Materials, Ministry of Education, Taiyuan University of Technology, Taiyuan, 030024, China. E-mail: lijie01@tyut.edu.cn.
b. Beijing Advanced Innovation Center for Materials Genome Engineering, Beijing Key Laboratory for Science and Application of Functional Molecular and Crystalline Materials, Department of Chemistry and Chemical Engineering, School of Chemistry and Biological Engineering, University of Science and Technology Beijing, Beijing 100083, China. E-mail: d202110468@xs.ustb.edu.cn.
c. Key Laboratory of Photochemical Conversion and Optoelectronic Materials, Technical Institute of Physics and Chemistry, Chinese Academy of Sciences, Beijing 100190, China. E-mail: zhengxie@mail.ipc.ac.cn.

General Remarks. Both reagents and solvents were obtained directly used as received from commercial companies without any pretreatment.

Characterizations. Powder X-ray diffraction (PXRD) was collected at room temperature on a PANalytical Empyrean series 3 diffractometer equipped with Cu Kα radiation operating at 45 kV and 40 mA and on a diffracted-beam graphite monochromator. X-ray photoelectron spectroscopy (XPS) data were conducted on an ESCALAB 250Xi system. Al *K*α X-ray (6 mA 12 kV) was utilized as the irradiation source. All measurements were performed in the CAE mode with the reference of C 1s (284.6 eV). The nitrogen adsorption and desorption isotherms were measured at 77 K using a Micromeritics ASAP 2020 PLUS HD88 system. The samples were degassed at 120 ℃ for 10.0 hours before the measurement. Scanning electron microscopy (SEM) images were performed on a HITACHI SU8010 microscope operated at an accelerating voltage of 10.0 kV. Transmission electron microscopy (TEM) images were acquired from a JEOL JEM 2100F and HT 7700 transmission electron microscopy. IR spectra were recorded as KBr pellets using a Bruker Tensor 37 spectrometer with 1.0 cm^{-1} resolution. The thermogravimetric analysis (TGA) curves were recorded on an SDT-Q600 instrument under a 40 mL min^{-1} N_2 flow at a heating rate of 10 ℃ min^{-1} within a temperature range of

40–800 ºC. The samples were pretreated at 120 ºC under dynamic vacuum to fully remove solvents trapped in the pores. UV–Vis absorption spectrum were obtained with a Cary 7000 (Varian, USA). The NLO properties at 532 nm were investigated by using a Z-scan setup (Nd: YAG laser, pulse duration: 3~6 ns, repetition rate: 10 Hz). Nanosecond transient absorption spectrum were performed using a commercial nanosecond laser flash photolysis spectrometer (LP980-KS, UK，repetition rate: 10 Hz, pulse duration: FWHM < 10 ns) at room temperature.

Density-Functional Theory Calculations. The molecular simulations were performed with gaussian 09 program[S1] using the PBE0 functional[S2] for all COF segment. The 6-31G(d) basis[S3] was chosen for C, H, N atoms, and SDD basis[S4] was chosen for Co atoms. The dispersion correction has been considered by using D3BJ.[S5] The selected COF fragments were shown in Figure S10 and S11.

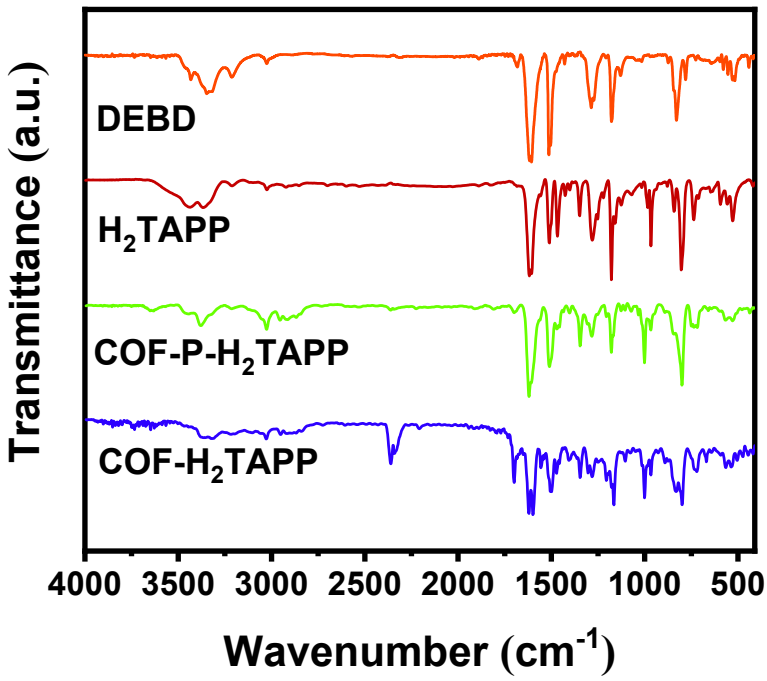

Figure S1. FT-IR spectra of **COF-H_2TAPP**, **COF-P-H_2TAPP** and respective starting materials (DEBD and H_2TAPP).

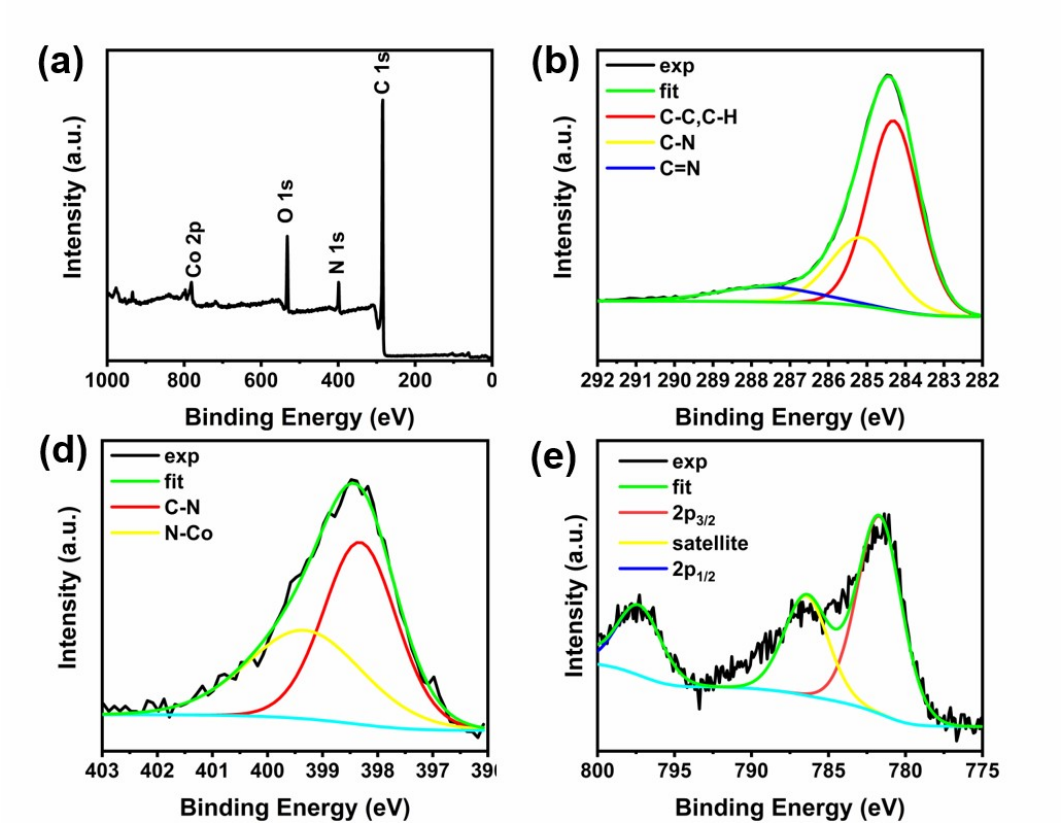

Figure S2. (a) The survey XPS of **COF-CoTAPP** and high-resolution spectra corresponding elements are (b) C 1s, (c) N 1s and (d) Co 2p, respectively.

Table S1 Atomic ratio of corresponding elements of **COF-CoTAPP**.

Element	Atomic %
C	89.42
N	8.33
Co	2.25

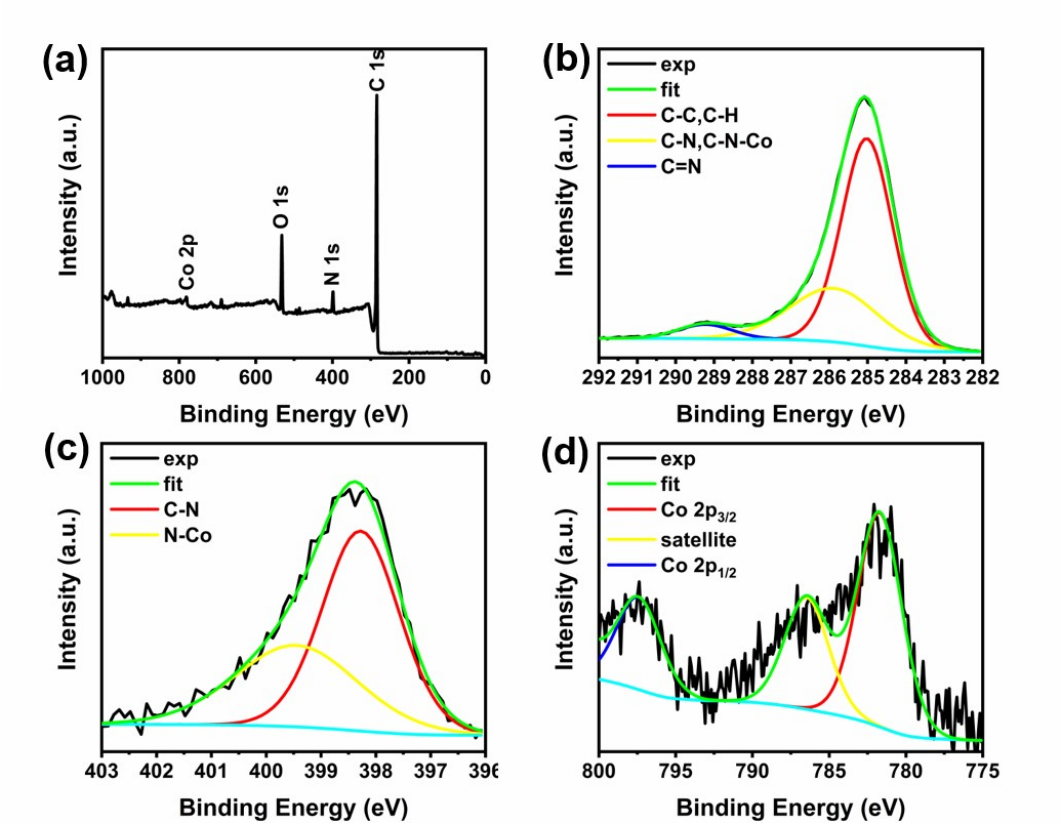

Figure S3. (a) The survey XPS of **COF-P-CoTAPP** and High-resolution spectra of corresponding elements are (b) C 1s, (c) N 1s and (d) Co 2p, respectively.

Table S2 Atomic ratio of corresponding elements of **COF-P-CoTAPP**.

Element	Atomic %
C	92.5
N	6.38
Co	1.12

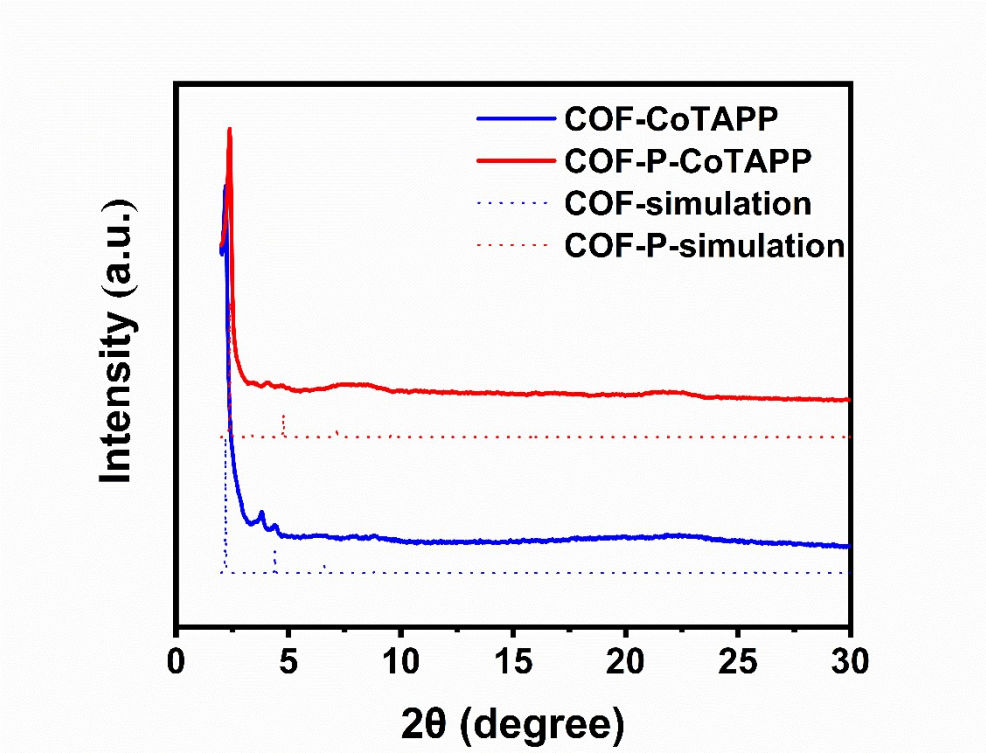

Figure S4. XRD patterns of **COF-CoTAPP** and **COF-P-CoTAPP**, experimentally observed (solid line) and simulated (dashed line).

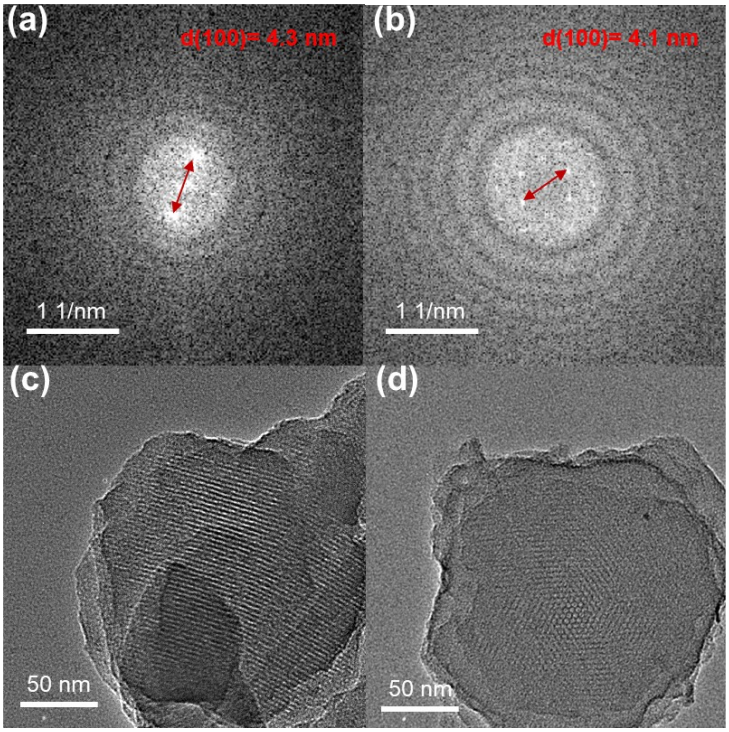

Figure S5. SEAD by Fast Fourier Transformation and TEM images of (a, c) **COF-H_2TAPP**, and (b, d) **COF-P- H_2TAPP**.

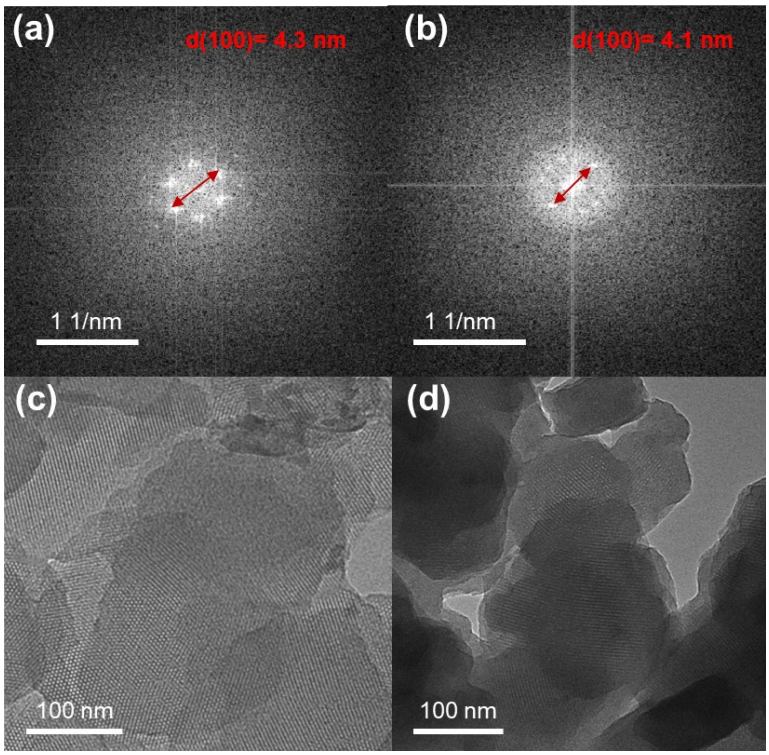

Figure S6. SEAD by Fast Fourier Transformation and TEM images of (a, c) **COF-CoTAPP** and (b, d) **COF-P-CoTAPP**.

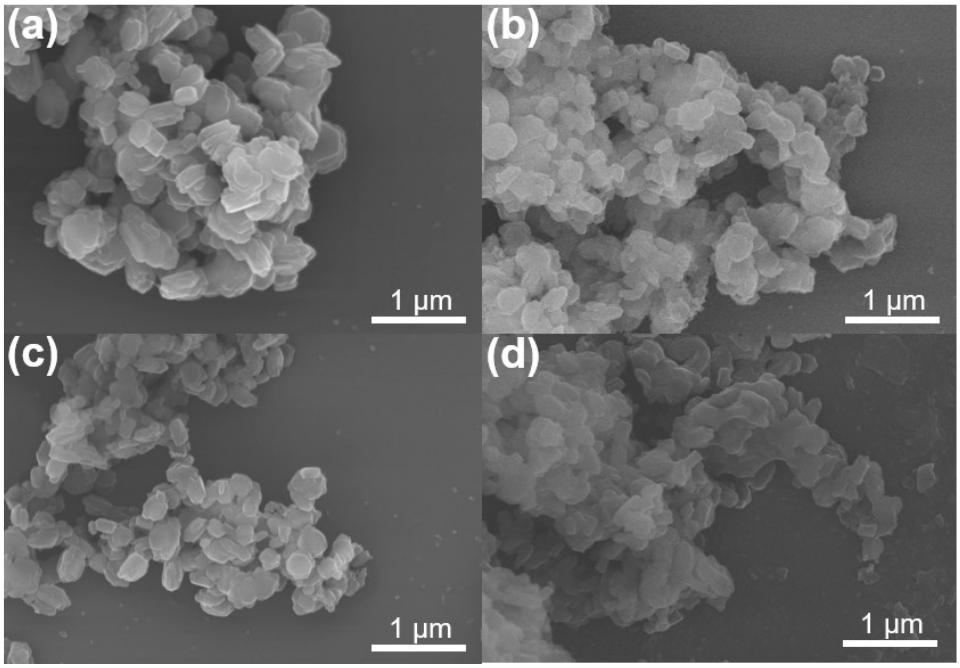

Figure S7. SEM images of (a) **COF-H_2TAPP**, (b) **COF-P-H_2TAPP**, (c) **COF-CoTAPP** and (d) **COF-P-CoTAPP**.

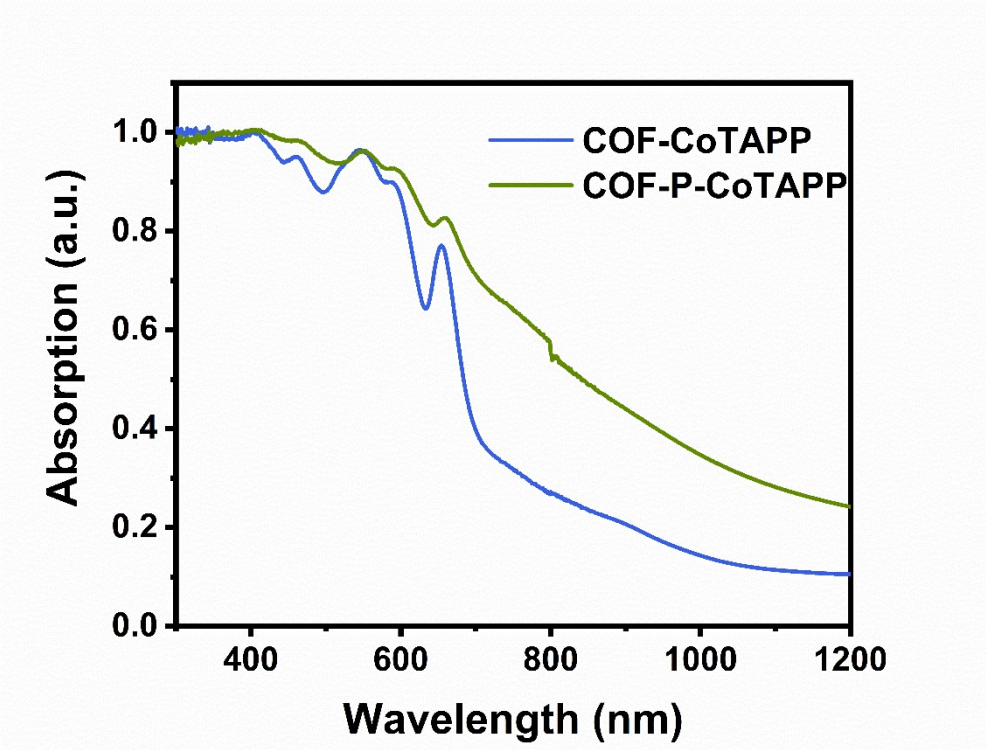

Figure S8. Solid UV-Vis absorption spectra of **COF-CoTAPP** and **COF-P-CoTAPP**.

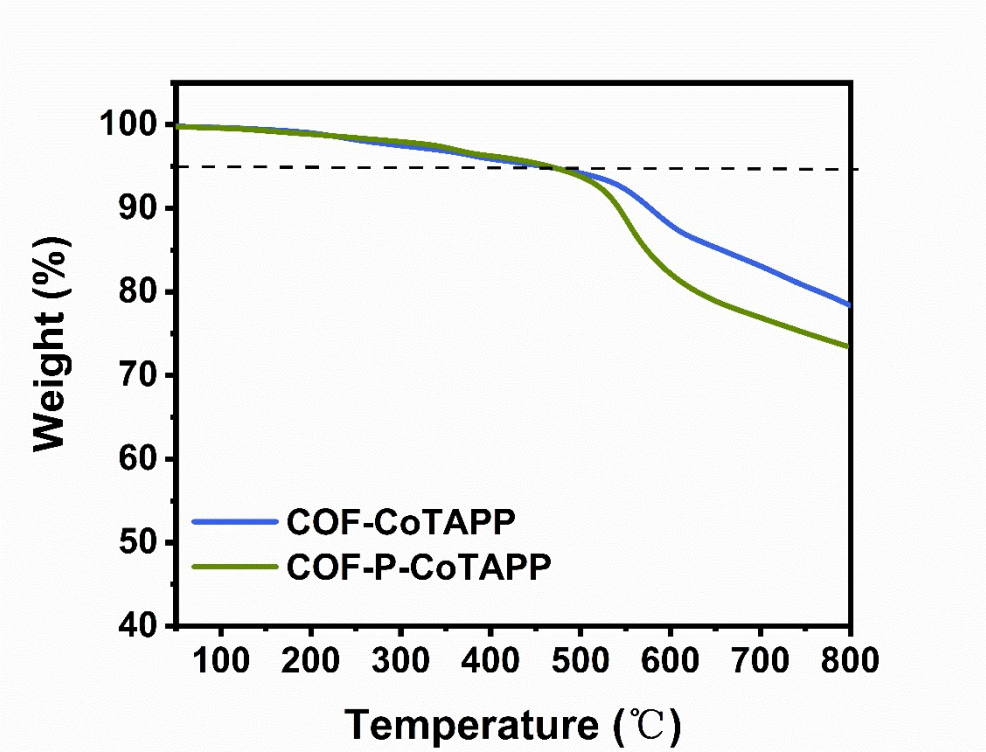

Figure S9. TGA curves of **COF-CoTAPP** and **COF-P-CoTAPP**.

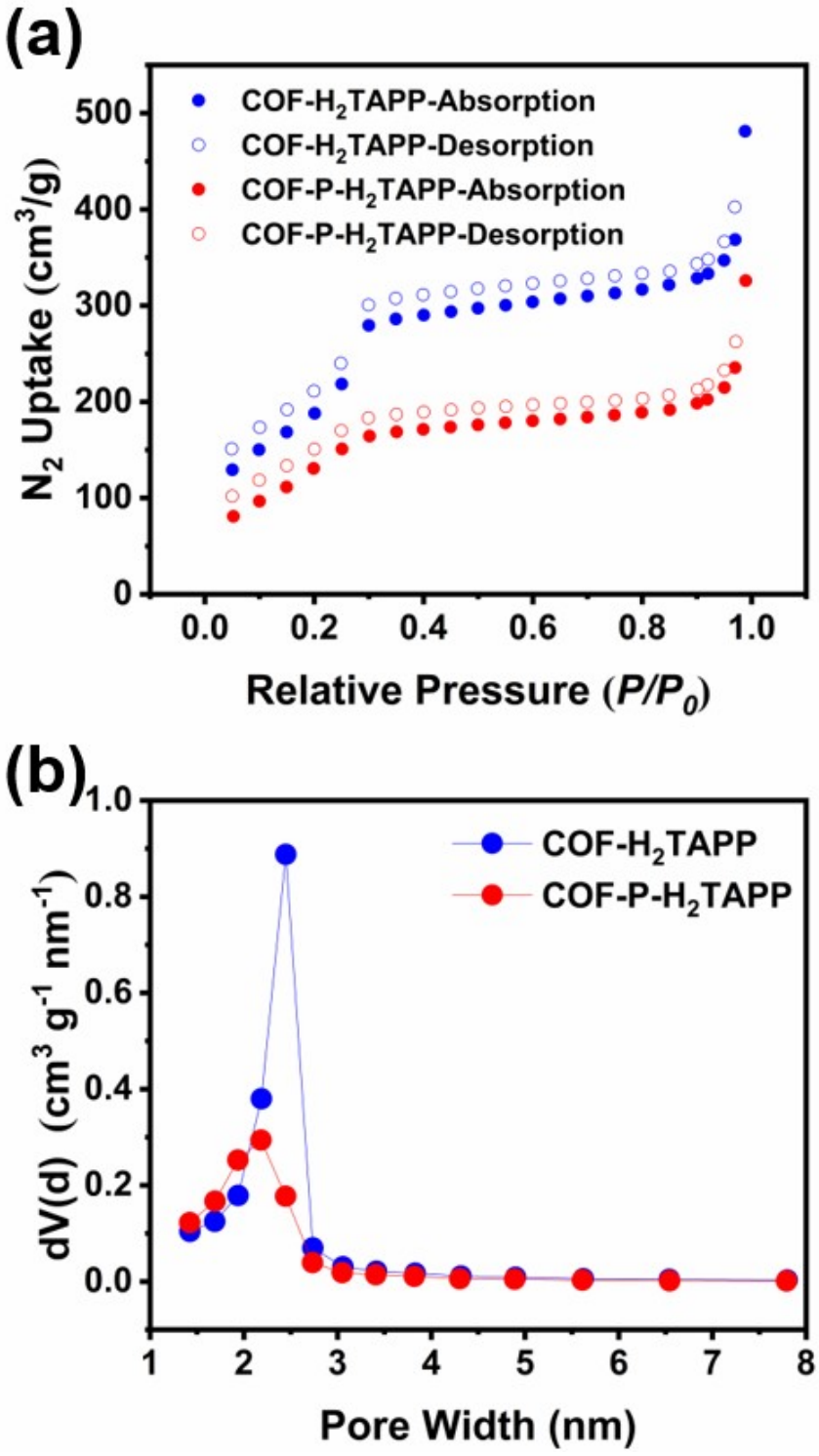

Figure S10. (a) N_2 sorption isotherms and (b) pore size distributions of **COF-H_2TAPP** and **COF-P-H_2TAPP**.

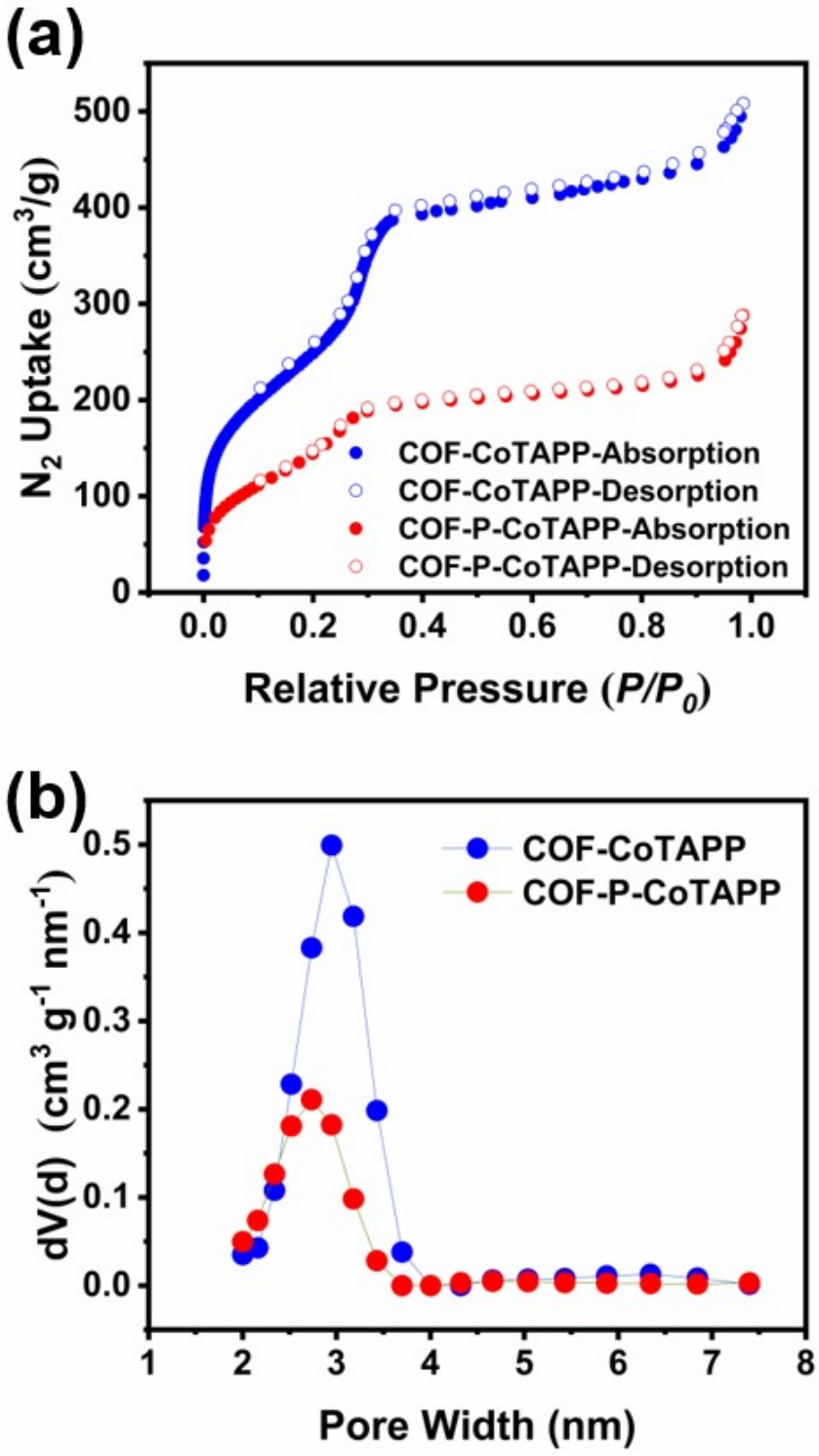

Figure S11. (a) N_2 sorption isotherms and (b) pore size distributions of **COF-CoTAPP** and **COF-P-CoTAPP**.

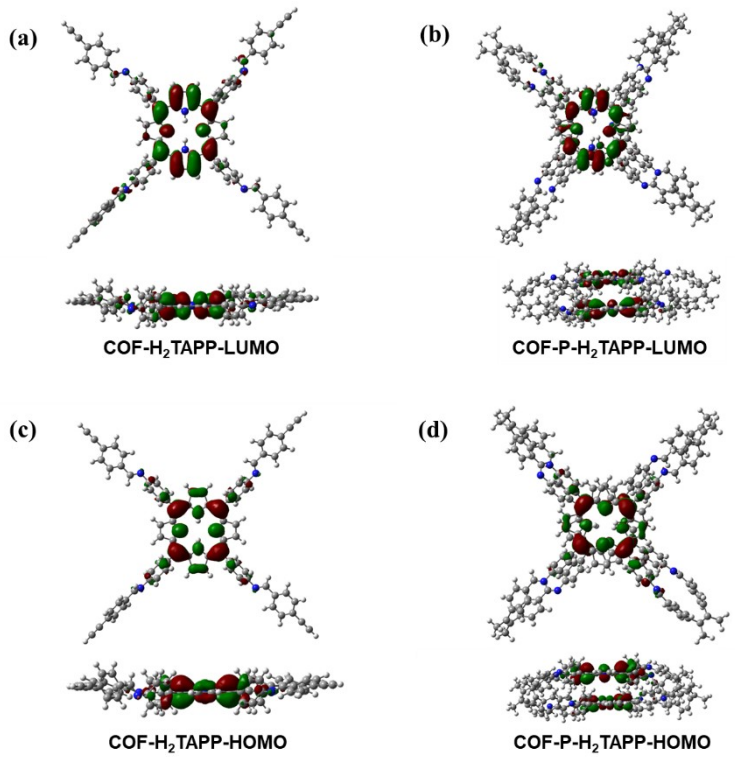

Figure S12. The isosurface of the electron wavefunction of the LUMO (a, b) and HOMO (c, d) of **COF-H_2TAPP** and **COF-P-H_2TAPP**.

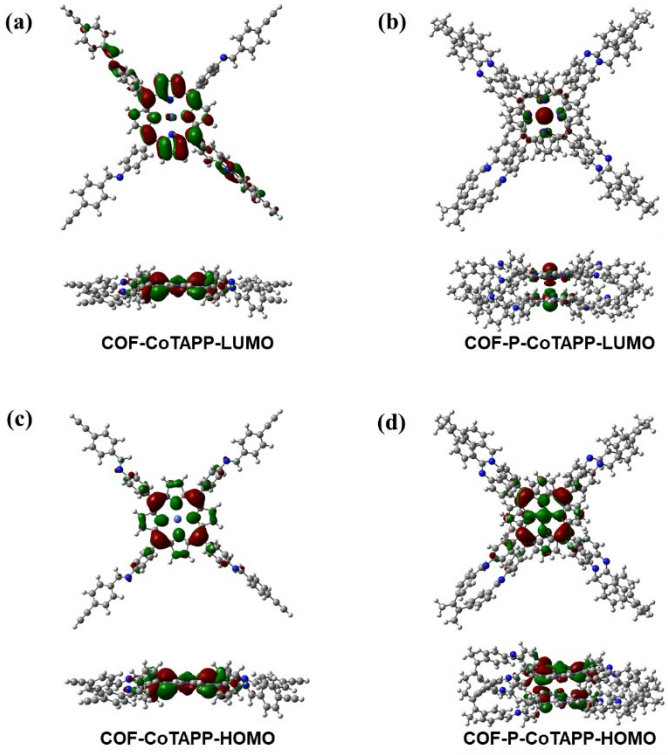

Figure S13. The isosurface of the electron wavefunction of the LUMO (a, b) and HOMO (c, d) of **COF-CoTAPP** and **COF-P-CoTAPP**.

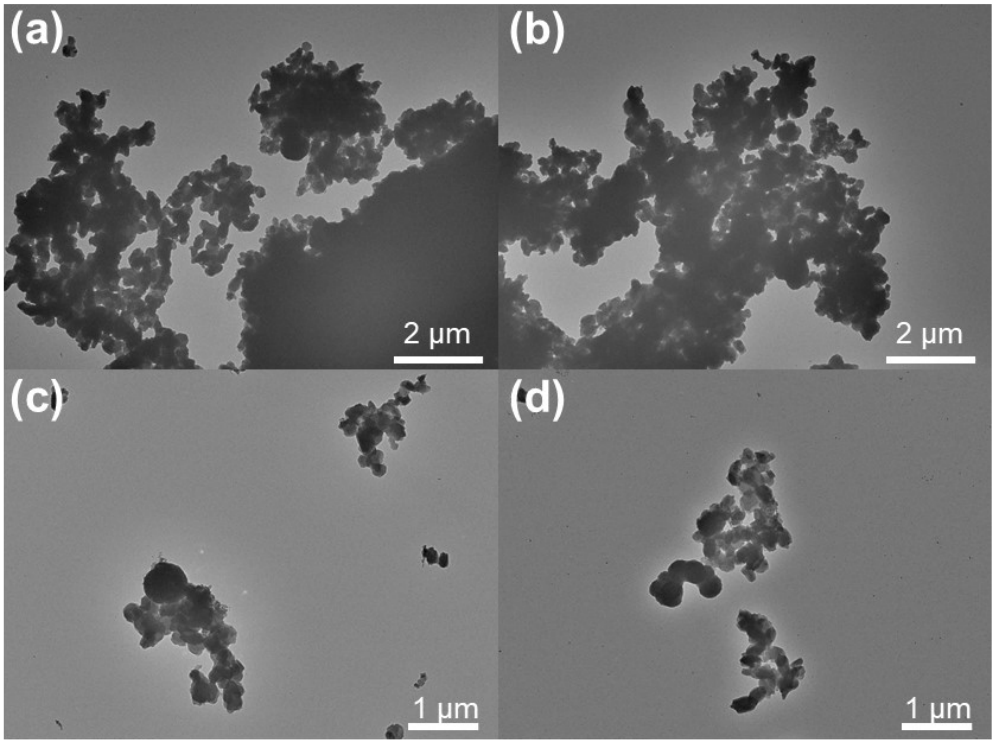

Figure S14. TEM images of **COF-H_2TAPP** and **COF-CoTAPP** before (a, b) and after (c, d) ultrasound.

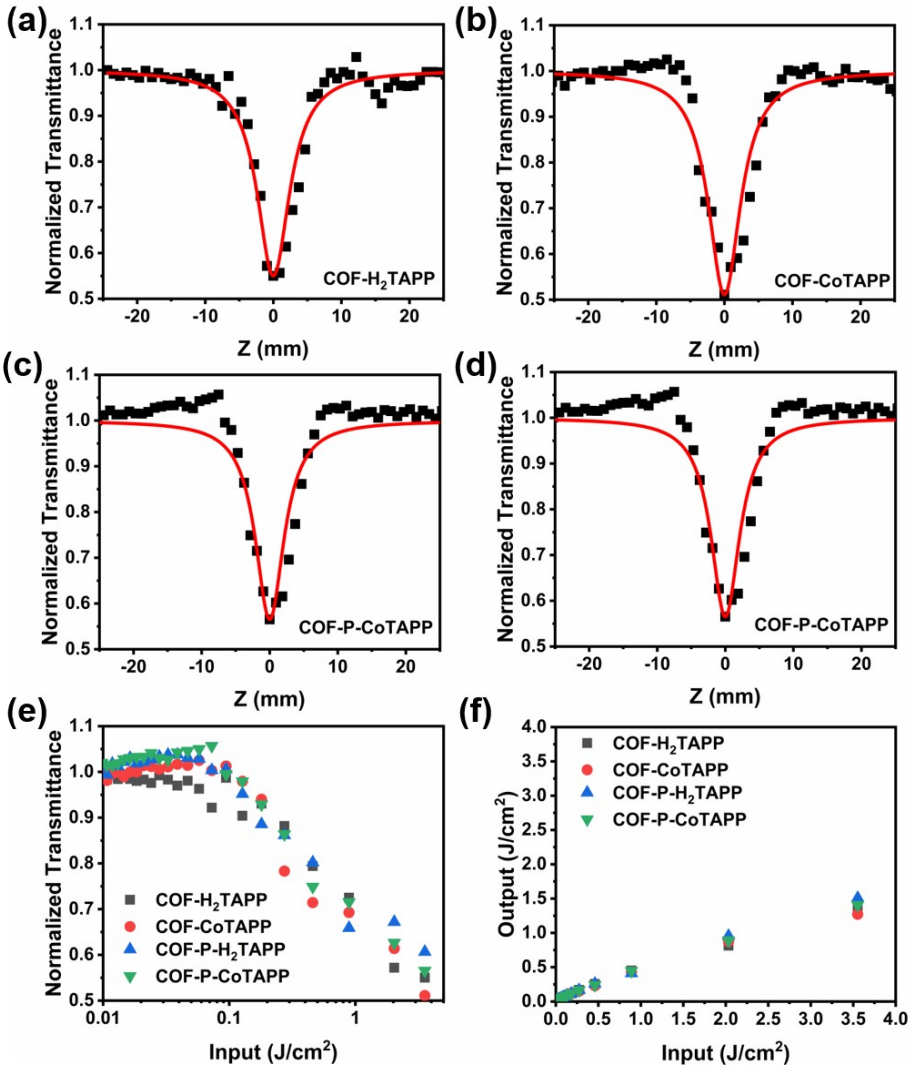

Figure S15. Normalized transmittance curves of open aperture Z-scan for **COF-MTAPP**, M = H_2 (a), Co (b), and **COF-P-MTAPP**, M = H_2 (d), Co (e) at 20.5 μJ. The solid lines represent the theoretical fitting, and the squares represent the experimental data. Input-normalized transmittance curves (c) and input-output energy density curves (f) of **COF-MTAPP** and **COF-P-MTAPP** by fit of Z-scan curves.

Fitting of the open aperture Z-scan curves and parameters calculation.

The open-aperture Z-scan curves can be fitted using the following equation based on the nonlinear optical model:[S6, S7]

$$T(z)=\sum_{m=0}^{\infty}\frac{(-q_0)^m}{(m+1)^{3/2}}\approx 1-\frac{\beta I_0 L_{eff}}{2\sqrt{2}\left(1+z^2/z_0^2\right)}=1-\frac{[1-T(z=0)]}{(1+z^2/z_0^2)}$$

Where T is the normalized transmittance, $z_0 = \pi\omega_0^2/\lambda$ is the Rayleigh diffraction length, z_0 and λ is

waist radius at focus and the wavelength of laser, L_{eff} is the sample's effective thickness, $L_{eff} = [1 - \exp(-\alpha_0 L)]/\alpha_0$, L is the sample thickness, $\alpha_0 = (-\ln T_0)/L$, α_0 is the linear absorption coefficient, T_0 is linear transmittance of the sample, I_0 is the input intensity on focus, β is the nonlinear absorption coefficient.

Table S3

A list of the nonlinear optical parameters of different porphyrin-based COFs.

Materials	Measurement condition	Nonlinear absorption coefficient	References
PorCOF-ZnNi	Z-scan, 532 nm, 6 ns	4170 cm/GW	S8
PorCOF-ZnCu	Z-scan, 532 nm, 6 ns	4470 cm/GW	S8
Por-TzTz-POF	Z-scan, 532 nm, 6 ns	1100 cm/GW	S9
COF-CoTAPP	Z-scan, 532 nm, 3~6 ns	38.80 cm/GW	This work

References

S1. C. Adamo and V. Barone, *J. Chem. Phys.,* 1999, **110**, 6158-6170.

S2. M. Frisch, G. W. Trucks, H. B. Schlegel, G. E. Scuseria, M. A. Robb, J. R. Cheeseman, G. Scalmani, V. Barone, B. Mennucci and G. Petersson, *Gaussian, Inc., Wallingford CT*, **2009**.

S3. a) P. C. Hariharan and J. A. Pople, *Theor. Chim. Acta,* 1973, **28**, 213-222; b) M. S. Gordon, *Chem. Phys. Lett.*, 1980, **76**, 163-168. c) R. C. Binning Jr, L. A. Curtiss, *J. Comput. Chem*., 1990, **11**, 1206-1216.

S4. D. Andrae, U. Haeussermann, M. Dolg, H. Stoll and H. Preuss, *Theor. Chim. Acta*, 1990, **77**, 123-141.

S5. S. Grimme, S. Ehrlich, L. Goerigk, *J. Comput. Chem.*, 2011, **32**, 1456-1465.

S6. S. Liu, Wang, S.. Yin, Z. Xie, Z. Wang, S. Zhou, P. Chen, *Phys. Status Solidi A*, 2019, **216**, 1800837

S7. R. Wei, X. Tian, L. Yang, D. Yang, Z. Ma, H. Guo and J. Qiu, *Nanoscale,* 2019, **11**, 22277-22285.

S8. B. P. Biswal, S. Valligatla, M. Wang, T. Banerjee, N. A. Saad, B. M. K. Mariserla, N. Chandrasekhar, D. Becker, M. Addicoat, I. Senkovska, R. Berger, D. N. Rao, S. Kaskel and X.

Feng, *Angew. Chem. Int. Ed.*, 2019, **58**, 6896-6900.

S9. M. Samal, S. Valligatla, N. A. Saad, M. V. Rao, D. N. Rao, R. Sahu and B. P. Biswal, *Chem. Commun.*, 2019, **55**, 11025-11028.

S10. Z. Liu, B. Zhang, Y. Huang, Y. Song, N. Dong, J. Wang and Y. Chen, *iScience*, 2021, **24**, 102526.